Use of the "shape-of-anomaly" data misfit in 3D inversion by planting anomalous densities

Leonardo Uieda and Valéria C. F. Barbosa, Observatório Nacional*

SUMMARY

We present an improvement to the method of 3D gravity gradient inversion by planting anomalous densities. This method estimates a density-contrast distribution defined on a grid of right-rectangular prisms. Instead of solving large equation systems, the method uses a systematic search algorithm to grow the solution, one prism at a time, around user-specified prisms called "seeds". These seeds have known density contrasts and the solution is constrained to be concentrated around the seeds as well as have their density contrasts. Thus, prior geologic and geophysical information are incorporated into the inverse problem through the seeds. However, this leads to a strong dependence of the solution on the correct location, density contrast, and number of seeds used. Our improvement to this method consists of using the "shape-of-anomaly" data-misfit function in conjunction with the ℓ_2-norm data-misfit function. The shape-of-anomaly function measures the different in shape between the observed and predicted data and is insensitive to differences in amplitude. Tests on synthetic and real data show that the improved method not only has an increased robustness with respect to the number of seeds and their locations, but also provides a better fit of the observed data.

INTRODUCTION

Methods for the 3D inversion of potential field data can be divided into two main categories: those that estimate the values of physical properties and those that estimate the form of the sources, given their physical property values. Examples from the category that estimates physical property values include Bear (1995), Li and Oldenburg (1998), and Portniaguine and Zhdanov (1999). The category that estimates the form of the sources can be subdivided into non-linear and linear methods. Non-linear methods generally parametrize the form of the sources using prisms with polygonal cross-section (e.g., Murthy and Swamy, 1996; Oliveira Jr et al., 2011) or polyhedra (e.g., Wildman and Gazonas, 2009). On the other hand, linear methods parametrize the subsurface using right rectangular prisms (e.g., Camacho et al., 2000; Krahenbuhl and Li, 2006; Silva Dias et al., 2009, 2011; Uieda and Barbosa, 2011). The method of Uieda and Barbosa (2011) implements a systematic search algorithm to iteratively "grow" the solution around user-specified prisms called "seeds". This method is based on the 2D approach of René (1986) and uses the regularizing function of Silva Dias et al. (2009) to impose compactness on the solution. The method is computationally efficient due to the implementation of a "lazy evaluation" of the sensitivity matrix. However, it is highly dependent on the number of seeds and the correct choice of their locations and density contrasts. We present an improvement to the method of Uieda and Barbosa (2011) which uses the "shape-of-anomaly" data-misfit function of René (1986) together with the traditional ℓ_2-norm data-misfit function. Tests on synthetic and real data show the improved robustness of our method with respect to the location and number of seeds.

METHODOLOGY

Let us assume that there are N_c types of observations available (e.g., the gravitational attraction and/or some combination of the components of the gravity gradient tensor). Now, let $\mathbf{g}^k$, $k = 1,\ldots,N_c$, be a vector with L observations of one of these types of data. We assume that $\mathbf{g}^k$ is caused by an anomalous density distribution in the subsurface. We discretize the subsurface into an interpretative model consisting of M juxtaposed right rectangular prisms with homogeneous densities. It follows that $\mathbf{g}^k$ can be approximated by the sum of the contribution of each prism. In matrix notation, this relation is given by

$$\mathbf{d}^k = \mathbf{A}^k\,\mathbf{p}, \tag{1}$$

where $\mathbf{d}^k$, $k = 1,\ldots,N_c$, is the L-dimensional predicted data vector, $\mathbf{p}$ is the M-dimensional parameter vector whose jth element is the density of the jth prism, and $\mathbf{A}^k$, $k = 1,\ldots,N_c$, is the $L \times M$ sensitivity matrix. The elements of the sensitivity matrix can be calculated using the formula of Nagy et al. (2000).

The misfit between $\mathbf{g}^k$ and $\mathbf{d}^k$ can be expressed through the normalized ℓ_2-norm data-misfit function

$$\phi^k(\mathbf{p}) = \sqrt{\frac{\sum_{i=1}^{L}\left(g_i^k - d_i^k\right)^2}{\sum_{i=1}^{L}\left(g_i^k\right)^2}}. \tag{2}$$

Another measure of this misfit is the "shape-of-anomaly" function of René (1986)

$$\psi^k(\mathbf{p}) = \sqrt{\sum_{i=1}^{L}\left(\alpha^k g_i^k - d_i^k\right)^2}, \tag{3}$$

where α^k, $k = 1,\ldots,N_c$, is a scale factor. The shape-of-anomaly function, as its name suggests, measures only the difference in shape between the observed and predicted data. If the two data have the same shape, they will differ only by a factor of α^k. Thus, the optimum value for α^k is the one that minimizes ψ^k (equation 3) (René, 1986). For a given predicted data vector $\mathbf{d}^k$ (equation 1), the value of α^k is calculated by differentiating ψ^k with respect to α^k and equating the result to zero, i.e.,

DOI http://dx.doi.org/10.1190/segam2012-0383.1

$$\frac{\partial \psi^k}{\partial \alpha^k} = \frac{\alpha^k \sum_{i=1}^{L} \left(g_i^k\right)^2 + \sum_{i=1}^{L} g_i^k d_i^k}{\sqrt{\sum_{i=1}^{L} \left(\alpha^k g_i^k - d_i^k\right)^2}} = 0\,. \tag{4}$$

Hence, before evaluating function ψ^k (equation 3), α^k can be calculated by (René, 1986)

$$\alpha^k = \frac{\sum_{i=1}^{L} g_i^k d_i^k}{\sum_{i=1}^{L} \left(g_i^k\right)^2}. \tag{5}$$

We can then define the total data-misfit function as the sum of the individual data-misfit functions (equation 2) of each type of data available, i.e.,

$$\Phi(\mathbf{p}) = \sum_{k=1}^{N_c} \phi^k(\mathbf{p}), \tag{6}$$

and, likewise, total shape-of-anomaly function as

$$\Psi(\mathbf{p}) = \sum_{k=1}^{N_c} \psi^k(\mathbf{p}). \tag{7}$$

From now on, we follow the methodology of Uieda and Barbosa (2011), in which the solution is iteratively built by the accretion of prisms to user-specified "seeds". These seeds are prisms of the interpretative model with given density contrasts. Before the iterative growth process starts, all elements of the parameter vector $\mathbf{p}$ are set to zero. Next, the elements of $\mathbf{p}$ corresponding to the seeds are assigned the density contrasts of the respective seeds (Figure 1a). The growth process is then started. An iteration of the growth process consists of attempting to grow, one at a time, each of the N_s seeds (Figure 1b). A seed grows by attempting to perform the accretion of one of its neighboring prisms (i.e., prisms that share a face). We define the accretion of a prism as changing its density contrast from zero to the density contrast of the respective seed undergoing the accretion. In order to be chosen for accretion, a neighboring prism must satisfy two criteria:

1. The accretion of a prism must decrease the total data-misfit function $\Phi(\mathbf{p})$ (equation 6) and satisfy the condition
$$\frac{|\Phi_{(new)} - \Phi_{(old)}|}{\Phi_{(old)}} \geq \delta, \tag{8}$$
where $\Phi_{(new)}$ is the value of $\Phi(\mathbf{p})$ evaluated with the prism included in the estimate, $\Phi_{(old)}$ is the previous value of $\Phi(\mathbf{p})$, and δ is a small positive constant that controls how much the solution is allowed to grow.
2. The accretion of a prism must produce the smallest value of the goal function $\Gamma(\mathbf{p})$ out of all other prisms that satisfy the first criterion. Unlike Uieda and Barbosa (2011), we define the goal function as
$$\Gamma(\mathbf{p}) = \Psi(\mathbf{p}) + \mu\theta(\mathbf{p}), \tag{9}$$
where $\Psi(\mathbf{p})$ is the total shape-of-anomaly function (equation 7), μ is a regularizing parameter, and $\theta(\mathbf{p})$ is a modified version of the regularizing function of Uieda and Barbosa (2011)
$$\theta(\mathbf{p}) = \frac{1}{f} \sum_{j=1}^{M} \frac{p_j}{p_j + \varepsilon} l_j, \tag{10}$$
where p_j, $j = 1, \ldots, M$, is the jth element of parameter vector $\mathbf{p}$, ε is a small positive constant, l_j is the distance between the jth prism and the seed which performed its accretion, and f is a scaling factor equal to the mean extent of the interpretative model (the region in the subsurface to be interpreted). In practice, ε is not needed because one could simply sum l_j or zero when evaluating the regularizing function.

If none of the neighboring prisms of a seed satisfy these criteria, the seed does not grow during this iteration. The growth process continues while at least one seed is able to grow (Figure 1c). Uieda and Barbosa (2012) provide an animation of a growth process performed on synthetic data using the method of Uieda and Barbosa (2011).

We emphasize that the full sensitivity matrices $\mathbf{A}^k$ are not needed at any single time during the inversion process. Therefore, the "lazy evaluation" of the sensitivity matrices proposed in Uieda and Barbosa (2011) is still possible in our modified algorithm, making the inversion fast and memory efficient.

For clarity, the modified planting algorithm proposed here will be henceforth referred to as the shape-of-anomaly planting algorithm.

APPLICATION TO SYNTHETIC DATA

We tested the advantages of the shape-of-anomaly planting algorithm over the method of Uieda and Barbosa (2011) on synthetic noise-corrupted data of the g_{zz} component of the gravity gradient tensor (Figure 2a-b). The synthetic data are produced by an elongated prismatic body with density contrast of 1.0 g/cm^3 (black frame in Figure 2c-d). The data set contains 400 observations on a regular grid at 150 meter height and were contaminated with pseudorandom Gaussian noise with zero mean and 2 Eötvös standard deviation. We applied both methods on this data set using an interpretative model consisting of 50,000 prisms. To yield adequate results, the method of Uieda and Barbosa (2011) would need several seeds correctly located along the strike of the source. However, here we used only one seed (white dot in Figure 2a-b) in both inversions. The depth of seed was 700 meters (center of the simulated body) for the method of Uieda and Barbosa (2011) and 300 meters (top of the simulated body) for the shape-of-anomaly planting algorithm. These values were the ones that yielded the best results for both methods. We used inversion control

DOI http://dx.doi.org/10.1190/segam2012-0383.1

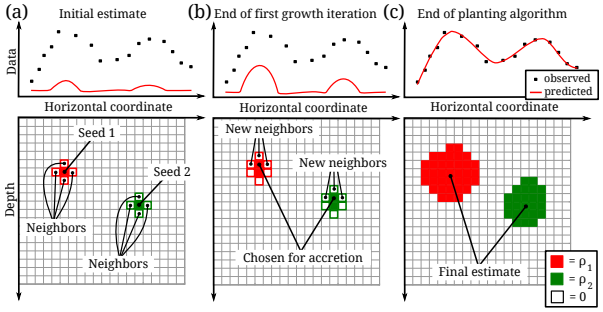

Figure 1: 2D sketch of three stages of the planting algorithm. In the upper panels, the black dots represent the observed data and the red line represents the predicted data produced by the current estimate. In the lower panels, the light gray grid of prisms represents the interpretative model, the color-filed prisms represent the current estimate, and the colored outlines represent the neighboring prisms of the current estimate. (a) Initial state with the user-specified seeds included in the estimate with their corresponding density contrasts and all other parameters set to zero. (b) End of the first growth iteration where two accretions took place, one for each seed. The neighboring prisms of each seed and the predicted data are updated. (c) Final estimate at the end of the algorithm. Modified from Uieda and Barbosa (2011).

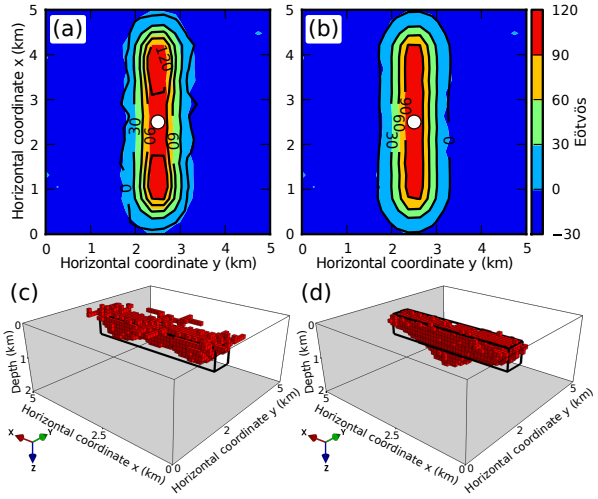

Figure 2: Application to synthetic data. (a-b) Synthetic noise-corrupted (colored contours) and predicted (black contour lines) g_{zz} components. White dots show the horizontal location of the seeds. (c-d) Perspective views of the estimated density-contrast distributions. a and c were produced by the method of Uieda and Barbosa (2011) and b and d by the shape-of-anomaly planting algorithm. Red prisms have density contrast of 1.0 g/cm^3. Prisms with density contrast of 0 g/cm^3 are not shown. The black prismatic frame in c and d is the outline of the true source.

variables $\mu = 10^5$ for Uieda and Barbosa (2011), $\mu = 0.2$ for shape-of-anomaly, and $\delta = 0.0005$ for both methods.

Figure 2c-d shows the estimated density-contrast distributions obtained using each method. As expected, the method of Uieda and Barbosa (2011) is not able to recover the correct geometry of the true source given only one seed. Moreover, the estimated density-contrast distribution (Figure 2c) is not entirely compact and the predicted data presents a reasonable fit to the synthetic data (Figure 2a). Conversely, the shape-of-anomaly planting algorithm estimates a density-contrast distribution (Figure 2d) that not only approximately recovers the geometry of the true source, but is fully compact and produces a better fit of the data.

APPLICATION TO REAL DATA

Quadrilátero Ferrífero

We applied the shape-of-anomaly planting algorithm to the gravity gradient data from the Quadrilátero Ferrífero, Brazil. We used the data of the g_{yz} and g_{zz} components in the inversion (Figure 3a) and assumed a density contrast of 1.0 g/cm^3 between the iron ore and the host rocks (Carlos et al., 2011; Uieda and Barbosa, 2011). The data set contains a total of 9164 measurements. The interpretative model consists of 310,500 prisms which follow the topography of the area. We used five seeds (white dots in Figure 3a) in the inversion, in contrast with the 46 seeds used by Uieda and Barbosa (2011). The inversion control variables were $\mu = 0.1$ and $\delta = 0.0001$. Figure 3b shows the estimated 3D density-contrast distribution. This estimate confirms that the geologic bodies are thin, compact, and elongated on the southwest-northeast direction. These results are in close agreement with previous interpretations by Martinez et al. (2010), Carlos et al. (2011) and Uieda and Barbosa (2011). The current estimate is, however, more compact than previous estimates, particularly in the southern parts. Figure 3a shows the fit between the observed and predicted data. Notice that the inversion fits the elongated southwest-northeast feature associated with the iron ore deposits.

Redenção granite

The Redenção granite is located in the Amazon Craton, northern Brazil. The residual Bouguer anomaly and the outline of the outcropping portion of the granite (red line) are shown in Figure 4a. We applied the shape-of-anomaly planting algorithm to the gridded gravity data set composed of 400 observations. The interpretative model consists of 215,040 juxtaposed prisms with approximate dimensions of $992 \times 1163 \times 166$ meters. Only one seed was used in the inversion (white dot in Figure 4a) at a depth of 3 km with density contrast of -0.09 g/cm^3 (Oliveira et al., 2008). We used inversion control variables $\mu = 0.5$ and $\delta = 5 \times 10^{-5}$. The estimated density-contrast distribution (Figure 4b-c) is compact and has an outcropping portion that is in agreement with the available geologic information (red line). The estimated granite has a sheet-like shape and thickness of approximately 6 km, which agrees with previous interpretations by Silva Dias et al. (2007) and Oliveira et al. (2008).

DOI http://dx.doi.org/10.1190/segam2012-0383.1

CONCLUSIONS

We have presented an improvement to the method of 3D inversion by planting anomalous densities. This method uses an iterative algorithm that builds the solution to the inverse problem through the accretion of prisms around user specified "seeds". Our improvement consists of modifying the goal function by exchanging the ℓ_2-norm data-misfit function by the "shape-of-anomaly" data-misfit function. The shape-of-anomaly function measures the difference in shape between the observed and predicted data, disregarding differences in amplitude. This exchange results in an improved fit of the observed data and increases the robustness of the method with respect to the number of seeds and correct choice of their depths. These improvements lead to a better delineation of elongated sources when providing a single seed. Tests on synthetic data and real gravity and gravity gradient data show the improved performance of our method in recovering compact geologic bodies.

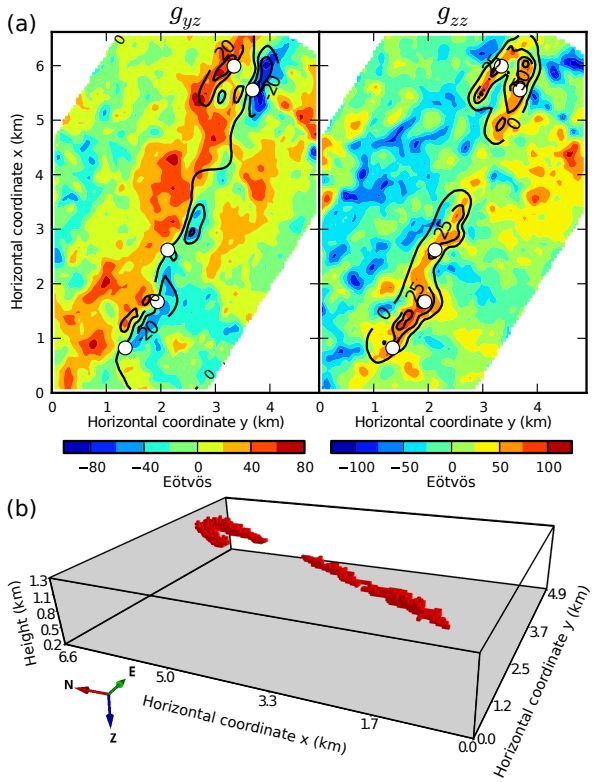

Figure 3: Application to gravity gradient tensor data from the Quadrilátero Ferrífero, Brazil. (a) Observed (colored contours) and predicted (black contour lines) g_{yz} and g_{zz} components of the gravity gradient tensor. White dots show the horizontal locations of the five seeds used in the inversion. (b) Perspective view of the estimated density-contrast distribution. Red prisms have density contrast of 1.0 g/cm^3. Prisms with density contrast of 0 g/cm^3 are not shown.

ACKNOWLEDGMENTS

We thank Vale for permission to use the data of the Quadrilátero Ferrífero. We acknowledge the use of software matplotlib by Hunter (2007) and Mayavi by Ramachandran and Varoquaux (2011) for 2D and 3D graphics, respectively. The authors were supported in this research by a fellowship (VCFB) from Conselho Nacional de Desenvolvimento Científico e Tecnológico (CNPq) and a scholarship (LU) from Coordenação de Aperfeiçoamento de Pessoal de Nível Superior (CAPES), Brazil. Additional support for the authors was provided by the Brazilian agencies CNPq (grant 471693/2011-1) and FAPERJ (grant E-26/103.175/2011).

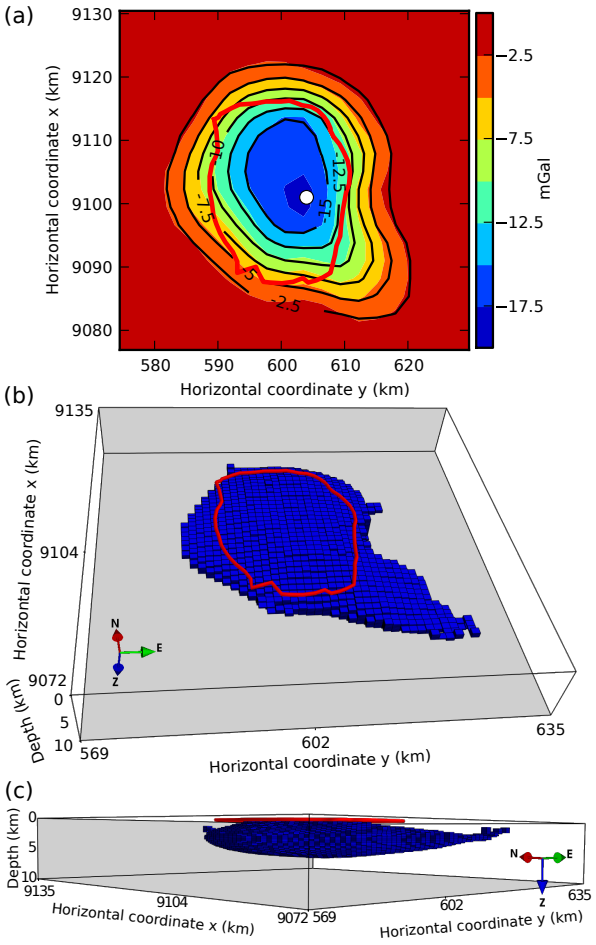

Figure 4: Application to the Bourguer anomaly data of the Redenção granite, Brazil. (a) Observed (colored contours) and predicted (black contour lines) data. The white dot shows the horizontal location of the single seed used in the inversion. (b-c) Perspective views of the estimated density-contrast distribution. Blue prisms have density contrast of -0.09 g/cm^3. Prisms with density contrast of 0 g/cm^3 are not shown. The red line in a-c represents the true outcropping portion of the pluton.

DOI http://dx.doi.org/10.1190/segam2012-0383.1

http://dx.doi.org/10.1190/segam2012-0383.1

EDITED REFERENCES

Note: This reference list is a copy-edited version of the reference list submitted by the author. Reference lists for the 2012 SEG Technical Program Expanded Abstracts have been copy edited so that references provided with the online metadata for each paper will achieve a high degree of linking to cited sources that appear on the Web.

REFERENCES

Bear, G. W., 1995, Linear inversion of gravity data for 3-D density distributions: Geophysics, **60**, 1354-1364, doi:10.1190/1.1443871.

Camacho, A. G., F. G. Montesinos, and R. Vieira, 2000, Gravity inversion by means of growing bodies: Geophysics, **65**, 95-101, doi:10.1190/1.1444729.

Carlos, D. U., L. Uieda, V. C. F. Barbosa, M. A. Braga, and A. A. S. Gomes, 2011, In-depth imaging of an iron orebody from Quadrilatero Ferrifero using 3D gravity gradient inversion: 81st Annual International Meeting, SEG, Expanded Abstracts, 902-906, doi:10.1190/1.3628219.

Hunter, J. D., 2007, Matplotlib: A 2D graphics environment: Computing in Science & Engineering, **9**, 90-95, doi: 10.1109/MCSE.2007.55.

Krahenbuhl, R. A., and Y. Li, 2006, Inversion of gravity data using a binary formulation: Geophysical Journal International, **167,** 543-556, doi:10.1111/j.1365-246X.2006.03179.x.

Li, Y., and D. W. Oldenburg, 1998, 3-D inversion of gravity data: Geophysics, **63**, 109-119, doi:10.1190/1.1444302.

Martinez, C., Y. Li, R. Krahenbuhl, and M. Braga, 2010, 3D Inversion of airborne gravity gradiomentry for iron ore exploration in Brazil: 80th Annual International Meeting, SEG, Expanded Abstracts, 1753-1757, doi:10.1190/1.3513181.

Murthy, I. R., and K. Swamy, 1996, Gravity anomalies of a vertical cylinder of polygonal cross-section and their inversion: Computers and Geosciences, **22**, 625-630, doi:10.1016/0098-3004(95)00126-3.

Nagy, D., G. Papp, and J. Benedek, 2000, The gravitational potential and its derivatives for the prism: Journal of Geodesy, **74,** 552-560, doi:10.1007/s001900000116.

Oliveira, D. C., R. Dall'Agnol, J. B. C. Silva, and J. A. C. Almeida, 2008, Gravimetric, radiometric, and magnetic susceptibility study of the Paleoproterozoic Redenção and Bannach plutons, eastern Amazonian Craton, Brazil: Implications for architecture and zoning of A-type granites: Journal of South American Earth Sciences, **25,** 100-115, doi:10.1016/j.jsames.2007.10.003.

Oliveira, Jr., V. C., V. C. F. Barbosa, and J. B. C. Silva, 2011, Source geometry estimation using the mass excess criterion to constrain 3-D radial inversion of gravity data: Geophysical Journal International, **187,** 754-772, doi:10.1111/j.1365-246X.2011.05172.x.

Portniaguine, O., and M. S. Zhdanov, 1999, Focusing geophysical inversion images: Geophysics, **64,** 874-887, doi:10.1190/1.1444596.

Ramachandran, P., and G. Varoquaux, 2011, Mayavi: 3D visualization of scientific data: Computing in Science and Engineering, **13**, 40-51, doi:10.1109/MCSE.2011.35.

René, R. M., 1986, Gravity inversion using open, reject, and "shape-of-anomaly" fill criteria: Geophysics, **51,** 988-994, doi:10.1190/1.1442157.

Silva Dias, F. J. S., V. C. F. Barbosa, and J. B. C. Silva, 2007, 3D gravity inversion incorporating prior information through an adaptive learning procedure: 77th Annual International Meeting, SEG, Expanded Abstracts, **26**, 745-749, doi:10.1190/1.2792521.

Silva Dias, F. J. S., V. C. F. Barbosa, and J. B. C. Silva, 2009, 3D gravity inversion through an adaptive-learning procedure: Geophysics, **74**, no. 3, I9–I21, doi:10.1190/1.3092775.

Silva Dias, F. J. S., V. C. F. Barbosa, and J. B. C. Silva, 2011, Adaptive learning 3D gravity inversion for salt-body imaging: Geophysics, **76**, no. 3, I49-I57, doi:10.1190/1.3555078.

Uieda, L., and V. C. F. Barbosa, 2011, Robust 3D gravity gradient inversion by planting anomalous densities: 81st Annual International Meeting, SEG, Expanded Abstracts, 820-824, doi:10.1190/1.3628201.

Uieda, L., and V. C. F. Barbosa, 2012, Animation of growth iterations during 3D gravity gradient inversion by planting anomalous densities: Figshare, http://hdl.handle.net/10779/2f26602b43f73723987b8d04946bfa41, accessed 01 April 2012.

Wildman, R. A., and G. A. Gazonas, 2009, Gravitational and magnetic anomaly inversion using a tree-based geometry representation: Geophysics, **74**, no. 3, I23-I35, doi:10.1190/1.3110042.

DOI http://dx.doi.org/10.1190/segam2012-0383.1